



Amplified signal response by cluster synchronization competition in rings with short-distance couplings

Xiaoming Liang ^{1,*} Lei Hua,¹ Xiyun Zhang,^{2,†} and Liang Zhao ³

¹*School of Physics and Electronic Engineering, Jiangsu Normal University, Xuzhou 221116, China*

²*Department of Physics, Jinan University, Guangdong 510632, China*

³*Department of Computer Science and Mathematics, University of São Paulo, Ribeirão Preto 14040-901, Brazil*



(Received 15 June 2022; accepted 23 November 2022; published 9 December 2022)

Topological resonance has been revealed in degree-heterogeneous scale-free networks for weak signal amplification, but not in degree-homogeneous all-to-all networks [Acebrón *et al.*, *Phys. Rev. Lett.* **99**, 128701 (2007)]. Here, we show that when the coupling distance of the all-to-all networks is reduced from global to local, i.e., converting all-to-all networks into rings, we can observe a resonant response to a weak signal similar to scale-free networks. We find that such a resonance effect induced by ring topology is robust across a wide range of ring sizes and signal frequencies. We further show that at intermediate coupling strength, oscillators in the rings can form separate synchronous clusters that compete with each other, resulting in large amplitude oscillations of boundary nodes between clusters and thus giving rise to the resonant signal amplification. Finally, we propose a structure of a three-node feed-forward motif simplified from the observed cluster synchronization competition to analyze the mechanism underlying the resonance behavior, which corresponds well with the numerical results.

DOI: [10.1103/PhysRevE.106.064306](https://doi.org/10.1103/PhysRevE.106.064306)

I. INTRODUCTION

Nature is full of nonlinear systems and signals, and the distinct response of these systems to diverse signals leads to a variety of observed phenomena [1–4]. Therefore, understanding how nonlinear systems respond to signals is important in multiple fields [5–9]. Due to its importance, numerous attempts have been devoted to exploring the mechanisms underlying the detection of weak signals in nonlinear systems. Stochastic resonance (SR) is a widely accepted mechanism with which nonlinear systems can amplify and detect weak signals by taking advantage of accompanying noise [10–12]. The mechanism of SR can be captured in an overdamped bistable oscillator, a nonlinear system with two stable states separated by a potential barrier [12–14]. When noise is too small, the bistable system vibrates at one of the two states and responds faintly to a weak input signal. In contrast, if noise is too large, the bistable system will switch between the two stable states at random, driven by the excessive noise overwhelming the signal. When noise is in an intermediate level, the switching events become regular and nearly synchronous with the signal. Thus, SR is a cooperative effect of random noise and weak signals.

Individual nonlinear systems are often connected to form networks [15–18]. Compared to a single-bistable system, the SR effect is dramatically improved in network-connected bistable systems [19–23]. This is known as array-enhanced SR, and its mechanism is from the dynamic feedback induced by coupling [19,20]. Moreover, different network

configurations also deeply affect the SR effect. For instance, small-world networks with a fraction of long-range shortcuts can enhance the performance of SR [24,25]; scale-free networks with a few highly connected hub nodes can generate a double SR [26,27]. Besides external noise, inherent disorder (quenched noise) originating from the units composing the ensemble may play a similarly constructive role of noise in optimizing the system response to weak signals. This effect is termed diversity-induced resonance [28]. Subsequent studies have shown that such a resonance effect is very general and appears in bistable, excitable, physical, and social systems, suggesting that diversity-induced resonance does not depend on the source of the disorder [29–31]. Recently, it was revealed that the heterogeneous topology of scale-free networks is a structural disorder that allows the networks to amplify weak signals without noise, i.e., topological resonance [32–34]. Specifically, in scale-free networks, most nodes (leaf nodes) have very few link connections (degrees), while a few nodes (hub nodes) have many connections, following a power-law degree distribution. Because of the heterogeneous connections, the collective driven from the leaf nodes assist the hub nodes in overcoming the potential barriers, leading to a resonant signal response in the hub nodes. Topological resonance, on the other hand, does not occur in degree-homogeneous all-to-all networks in which all nodes have the same degree with a delta functionlike degree distribution, and no source of disorder exists in this case [32]. This finding raises the question whether a resonance effect of signal amplification can be observed in degree-homogeneous networks and, if so, what kind of network is appropriate and where the disorder comes from.

In this paper, we show that an equivalent weak signal amplification can be obtained in degree-homogeneous rings.

*xmliang@jsnu.edu.cn

†xiyunzhang@jnu.edu.cn

We construct a network in which the nodes are arranged as a ring. By reducing the coupling distance, the network can be changed from an all-to-all topology (as in Ref. [32]) to a ring structure (nearest-neighbor coupling). We observe a resonance behavior, i.e., the maximum response of the ring to a weak signal appears for intermediate coupling strength, analogous to scale-free networks. Through extensive tests, we demonstrate that this resonance effect is robust for various ring sizes and signal frequencies. Further, we find that cluster synchronization and the competition between different clusters underlie the observed resonance behavior. At last, this resonance behavior is analyzed utilizing a three-node feed-forward motif.

II. MODEL

We consider a regular ring of N identical bistable units, each of which is connected to R nearest neighbors, and subjected to the same external periodic signal. The corresponding dynamics of the units are

$$\dot{x}_i = x_i - x_i^3 + \lambda \sum_{j=i-R}^{j=i+R} (x_j - x_i) + A \sin(\omega t), \quad i = 1, \dots, N, \quad (1)$$

where $\lambda \geq 0$ is the coupling strength, and $R \in [1, N/2]$ is the coupling distance. The interaction between units is limited to the nearest neighbors (local coupling) for $R = 1$ and all-to-all (global coupling) for $R = N/2$; thus, the intermediate distances $0 < R < N/2$ correspond to the intermediate couplings. A and ω are the intensity and frequency of the external signal, respectively. A single isolated unit ($\lambda = 0$) vibrates slightly around one of its two stable fixed points $x_s = \pm 1$ when A is small (subthreshold). In contrast, it oscillates significantly around its unstable fixed point $x_u = 0$ when A is large (suprathreshold). The transition from small-amplitude vibration to large-amplitude oscillation occurs discontinuously at $A_c = \sqrt{4/27}$ for low ω [13,35]. However, there is no apparent threshold intensity A_c for high ω , as the transition becomes continuous with A [36]. This study aims to explore whether a resonance effect of signal amplification can appear in degree-homogeneous networks taking the regular ring as a testing example, where both coupling distance and strength are considered key parameters.

Since all units oscillate at the same frequency following the external periodic signal, we may characterize their dynamics by the oscillating amplitudes

$$g_i = \frac{\max x_i - \min x_i}{2}, \quad (2)$$

and the centers

$$c_i = \frac{\max x_i + \min x_i}{2}. \quad (3)$$

According to Eq. (2), we define the response of the ring in terms of the maximum amplitude of the units [32,33]:

$$G = \frac{gL}{A}, \quad (4)$$

where L signifies the index of the unit with the largest amplitude, i.e., $g_L = \max_{i=1}^N g_i$. $G > 1$ and $G < 1$ correspond to amplified signal response and damped signal response,

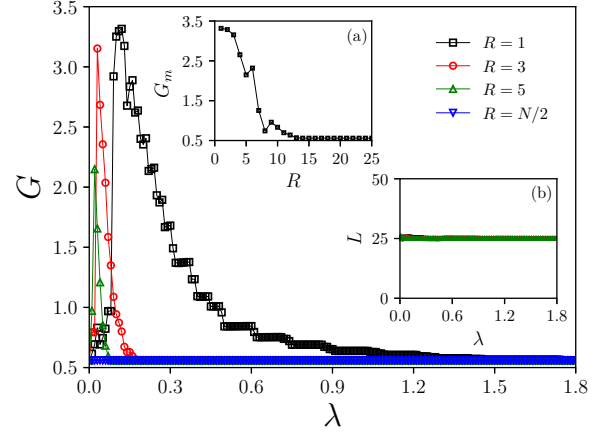


FIG. 1. Signal response G versus coupling strength λ for coupling distance $R = 1, 3, 5, N/2$. Insets: (a) resonance peak G_m versus coupling distance R , (b) average index L versus coupling strength λ . Parameters $N = 50$, $A = 0.3$, and $\omega = 2\pi/50$ are considered.

respectively. Since network function is closely related to network synchronization [37–39], we define an order parameter ρ to measure the coherence of the units in the ring [40,41]:

$$\rho = \frac{1}{2RN} \left\langle \sum_{i=1}^N \sum_{j=i-R}^{j=i+R} H(x_i x_j) \right\rangle_t, \quad (5)$$

where $\langle \cdot \rangle$ is the average over time and $H(\cdot)$ is the Heaviside step function that returns zero for negative input and one for nonnegative input. The ring is fully asynchronous with $\rho = 0.5$ when all units vibrate randomly about different centers $x_s = \pm 1$ since the probability of two adjacent units vibrating around the same center is 0.5. Instead, the ring is synchronous with $\rho = 1$ when all units vibrate around the same center $x_s = 1$ or $x_s = -1$.

In numerical simulations, the initial states of the bistable units are chosen randomly from $x_s = \pm 1$; the obtained signal response G and order parameter ρ are averaged over 1000 realizations with different initial states.

III. SIMULATIONS

We start from a fully connected ring, i.e., an all-to-all network. Consider a ring of bistable units with $N = 50$ and $R = N/2$ forced by a subthreshold signal with $A = 0.3$ and $\omega = 2\pi/50$. As shown in Fig. 1, the ring generates a constant response ($G \approx 0.5$) to the subthreshold signal, consistent with the finding in [32]. This damped response is because all units in the ring are fully synchronized with $\rho = 1$, even for tiny coupling strength $\lambda \approx 0$ [see Fig. 2]. Thus, the all-to-all network behaves as a single isolated unit [i.e., Eq. (1) with $\lambda = 0$], producing a damped signal response. With the reduction of coupling distance R , the all-to-all network gradually becomes a ring, and the response to the subthreshold signal is also shown in Fig. 1. For local coupling ($R = 1$), the signal response G is significantly amplified ($G > 1$) at intermediate coupling strength, exhibiting the typical feature of resonance. For intermediate coupling ranges ($R = 3$ and $R = 5$), the resonance effect gradually fades, i.e., the resonance peak

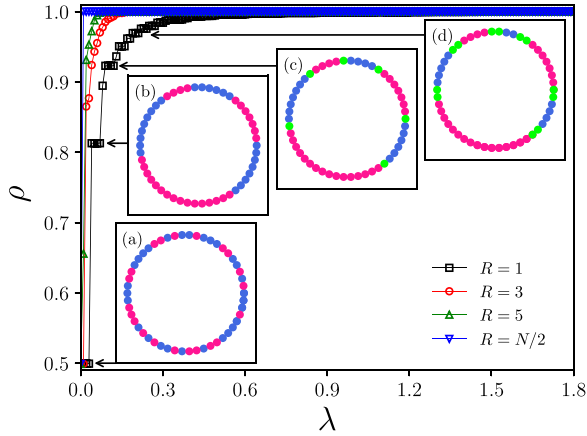


FIG. 2. Order parameter ρ versus coupling strength λ for coupling distance $R = 1, 3, 5, N/2$ (with the same parameters used in Fig. 1). Insets (a)–(d) are the typical partial synchronization patterns of the ring in the synchronization process, where solid pink circles represent cluster I, in which the units vibrate around $x_s = 1$, solid blue circles represent cluster II, in which the units vibrate around $x_s = -1$, and solid cyan circles represent cluster III, in which the units oscillate around $x_u = 0$.

G_m falls, and the coupling interval for signal amplification ($G > 1$) also shrinks. The signal response G changes from signal amplification ($G_m > 1$) to degradation ($G_m < 1$) [see the inset (a) in Fig. 1] with a further increase of the coupling distance. Meanwhile, the average index of the unit with the largest amplitude remains constant at a value close to $L \approx N/2$ [see the inset (b) in Fig. 1]. These observations demonstrate that the resonance effect of signal amplification can occur in degree-homogeneous rings with short-distance couplings, and all units in the rings have an equal chance to be the resonator (with the maximum signal response).

Figure 2 shows the order parameter ρ corresponding to the signal response G as described in Fig. 1. For all-to-all coupling ($R = N/2$), the onset of complete synchronization $\rho = 1$ occurs at $\lambda_c \approx 0$. For intermediate and local couplings, the critical coupling strength λ_c increases as R decreases and reaches the maximum when $R = 1$. These different values of λ_c for complete synchronization correspond to the various coupling intervals for signal amplification shown in Fig. 1. Taking the local coupling ($R = 1$) as an example, the insets in Fig. 2 illustrate four typical partial synchronization patterns in the path to complete synchronization. For a tiny coupling strength, the units are distributed randomly around two centers $x_s = \pm 1$ [see inset (a) in Fig. 2]. When the coupling strength exceeds $\lambda_1 = 0.04$, the units synchronize with adjacent neighbors, forming two synchronization clusters [see inset (b) in Fig. 2]. The first (cluster I) is composed of the units that vibrate around $x_s = 1$, whereas the second (cluster II) is composed of the units that vibrate around $x_s = -1$. Each cluster is not spatially consecutive, but alternates along the ring. With an even stronger coupling $\lambda_2 = 0.09$, the units at the cluster boundaries begin to hop back and forth between clusters I and II [see inset (c) in Fig. 2]. They gradually grow in size to form the third type of cluster (cluster III) with the increase of coupling strength [see inset (d) in Fig. 2]. However, excessive

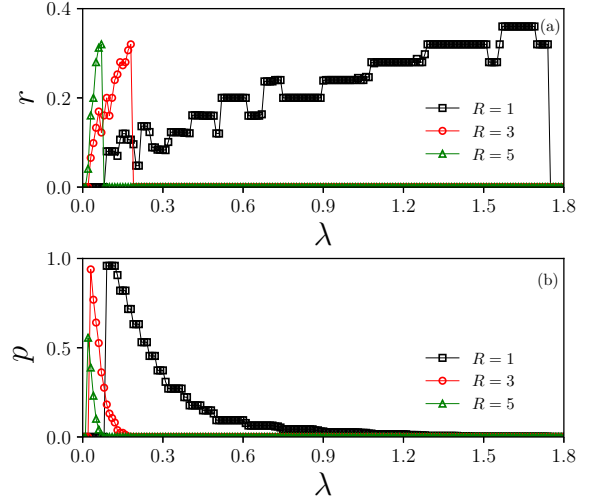


FIG. 3. Scale ratio r of cluster III to the ring in (a) and success rate p of forming cluster III in (b) versus coupling strength λ for coupling distance $R = 1, 3, 5$. Parameters are the same as in Fig. 1.

coupling strength eventually causes the ring to attain complete synchronization. Accordingly, neither asynchronization ($\rho = 0.5$) nor complete synchronization ($\rho = 1$) benefits signal amplification, and only cluster synchronization (partial synchronization) $0.5 < \rho < 1$ enhances the amplification of weak signal.

To investigate the dynamic details, we calculate and show in Fig. 3(a) the scale ratio $r = N_0/N$ describing the proportion of cluster III as a function of the coupling strength λ , where N_0 stands for the number of units belonging to cluster III. We set a threshold $\theta = 0.1$ and consider the unit in cluster III when its oscillating center $|c_i| \leq \theta$. Figure 3(a) shows that the scale ratio r rises from $r = 0$ to $r \approx 1/3$ when the coupling strength λ increases to λ_c ; after this peak, the scale ratio returns to $r = 0$ as the ring attains complete synchronization. Furthermore, the coupling interval for $r > 0$ reduces as the coupling distance R increases. Figure 3(b) shows the success rate p of forming cluster III (i.e., $r > 0$) over many realizations. By comparing Figs. 3(a) and 3(b), the success rate p steadily decreases as λ and R increase, indicating that cluster III of small scale ($r \approx 1/10$) is more general in rings than large scale ($r \approx 1/3$).

Figure 4 presents the robustness of the resonance effect observed in rings with short-distance couplings for various ring sizes and signal frequencies. As shown in Fig. 4(a), the signal response of the ring with local coupling is resonant for both small and large N . The height of the resonance peak G_m and its width (the width of the peak at half height) increase with N . This is due to the fact that a larger ring requires a stronger coupling to establish synchronization. Figure 4(b) shows that the resonance peak G_m saturates at large N , and the saturation rate decreases with increasing the coupling distance R . This is because a large coupling distance R enables the ring to synchronize, reducing the signal response of cluster III. Similarly, the ring with local coupling generates the resonant signal response for various signal frequencies, see Fig. 4(c). As ω lowers, the height of the resonance peak G_m grows, while the peaks width decreases. Moreover, as seen in Fig. 4(d), the resonance peak G_m saturates at low ω , and this trend holds true

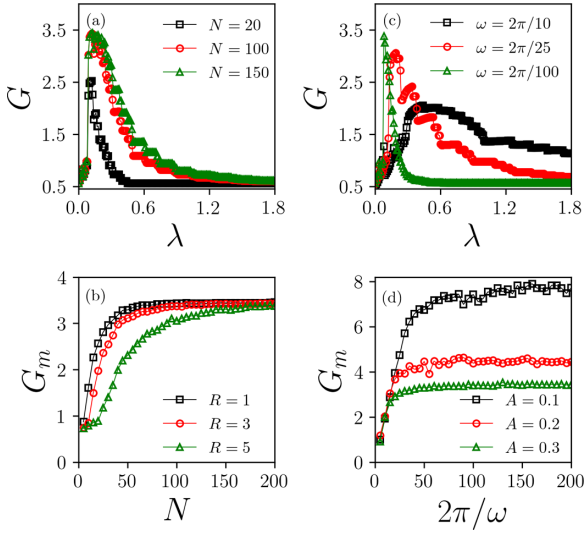


FIG. 4. (a) Signal response G versus coupling strength λ for ring size $N = 20, 100, 150$, with fixed $A = 0.3$, $\omega = 2\pi/50$, and $R = 1$. (b) Resonance peak G_m versus ring size N , with fixed $A = 0.3$ and $\omega = 2\pi/50$. (c) Signal response G versus coupling strength λ for signal frequency $\omega = 2\pi/10, 2\pi/25, 2\pi/100$, with fixed $A = 0.3$ and $R = 1$. (d) Resonance peak G_m versus signal frequency ω , with fixed $N = 50$ and $R = 1$.

for different signal intensities. Note that the low G_m at high ω results from cluster III oscillating too quickly and avoiding wide-range jumps. These features imply that the resonance effect of signal amplification in degree-homogeneous rings is robust to ring size and signal frequency.

IV. ANALYSIS

To give an analytical insight into our findings, we consider the simple case of the ring with local coupling $R = 1$. As seen in Fig. 2, the ring with local coupling evolves via a two-step process of cluster synchronization for signal amplification. The first step occurs at $\lambda < \lambda_1$, where the ring tends to form two-cluster partial synchronization; the second happens at $\lambda \geq \lambda_1$, and the ring develops into three-cluster partial synchronization. During these two-step synchronization processes, the ring can be simplified by a feed-forward motif composed of three bistable units [42–44]:

$$\begin{aligned} \dot{y}_1 &= y_1 - y_1^3 + A \sin(\omega t), \\ \dot{y}_2 &= y_2 - y_2^3 + A \sin(\omega t), \\ \dot{y}_3 &= y_3 - y_3^3 + \lambda(y_1 + y_2 - 2y_3) + A \sin(\omega t), \end{aligned} \quad (6)$$

where units one and two are the nearest neighbors of unit three who have separately joined clusters I and II and attempt to absorb unit three. Thus, units one and two have more stable dynamics, while unit three has less influence on them. Given this, the three units form a feed-forward motif, and the ring with local coupling can be regarded as a collection of three-node feed-forward motifs.

Figure 5 compares the signal response of the feed-forward motif to the ring with $N = 50$ and $R = 1$. When $\lambda < \lambda_2$, the motif provides a nearly equal signal response to the ring; and when $\lambda \geq \lambda_2$, it shows a qualitatively similar tendency

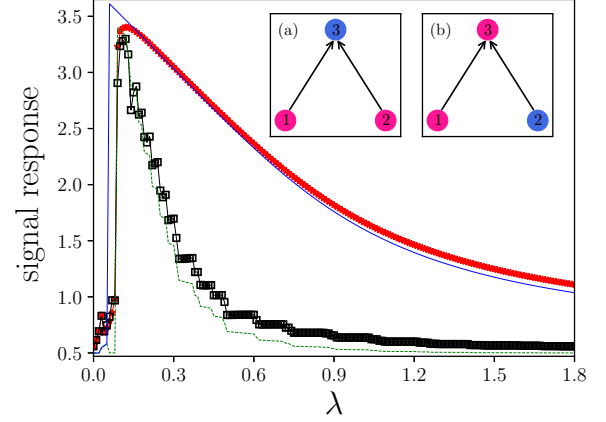


FIG. 5. Signal responses G , G_{motif} , and G_{ring} , as a function of the coupling strength λ . Black squares denote the numerical G of the ring with $N = 50$ and $R = 1$, red circles denote the numerical G of the feed-forward motif, blue solid line denotes the analytical G_{motif} , and green dotted line denotes the analytical G_{ring} . Insets (a) and (b) are two schematic sketches of the feed-forward motif for $\lambda < \lambda_1$ and $\lambda_1 \leq \lambda < \lambda_2$, respectively. Subthreshold periodic signal of $A = 0.3$ and $\omega = 2\pi/50$ is considered.

of the signal response of the ring. The disparity at $\lambda \geq \lambda_2$ is due to two factors: (i) the interactions between units in the feed-forward motif are unidirectional, but they are bidirectional in the ring; and (ii) the signal response becomes more sensitive to the initial state of the ring as the coupling strength increases while the feed-forward motif is not [see Fig. 3(b)]. Nonetheless, the simple feed-forward motif captures the essential characteristic of the resonancelike signal response of the ring and has the advantage of being solvable. In the following, we use the feed-forward motif to analyze the mechanism of the resonant response of the ring with $R = 1$.

A. Case I: $\lambda < \lambda_1$

Inset (a) in Fig. 5 gives a schematic sketch of the feed-forward motif for $\lambda < \lambda_1$, with units one and two oscillating around the same center $x_s = 1$, and unit three oscillating around the other center of $x_s = -1$. Since units one and two are isolated in the feed-forward motif and the signal intensity A is subthreshold, we may use the linearization method to determine their solutions, which are

$$y_{1,2}(t) = x_s + \frac{2A}{4 + \omega^2} \sin(\omega t) - \frac{\omega A}{4 + \omega^2} \cos(\omega t). \quad (7)$$

As mentioned earlier, the signal response of the ring with global coupling is equal to that of an isolated unit when $\lambda > 0$; so Eq. 7 yields

$$G_{\text{global}} = G_{\text{single}} = \frac{1}{\sqrt{4 + \omega^2}}, \quad (8)$$

which is a damped signal response and is independent of the coupling strength λ .

Because units one and two are in the same cluster, i.e., $y_1 = y_2$, the dynamics of unit three becomes as follows:

$$\dot{y}_3 = (1 - 2\lambda)y_3 - y_3^3 + 2\lambda + AB \sin(\omega t + \phi_1), \quad (9)$$

where $B = \sqrt{(4\lambda + 4 + \omega^2)^2 + 4\omega^2\lambda^2}/(4 + \omega^2)$ and ϕ_1 denotes the phase shift. In Eq. (9), the periodic signal $AB \sin(\omega t + \phi_1)$ changes from subthreshold to suprathreshold as the coupling strength exceeds a threshold coupling strength λ'_1 , satisfying [35]

$$\left(\frac{2R\lambda'_1 + AB}{2}\right)^2 = \left(\frac{1 - 2R\lambda'_1}{3}\right)^3. \quad (10)$$

For $A = 0.3$ and $\omega = 2\pi/50$, the threshold $\lambda'_1 \approx 0.025$ which nears the numerical result $\lambda_1 = 0.04$ for the ring with $R = 1$. Accordingly, the signal $AB \sin(\omega t + \phi_1)$ is subthreshold when $\lambda < \lambda'_1$, and we may solve Eq. (9) by the linearization method, yielding

$$y_3(t) = x_s + \frac{AB}{\sqrt{4(1 + \lambda)^2 + \omega^2}} \sin(\omega t + \phi_2), \quad (11)$$

where ϕ_2 denotes some phase shift. Equation (11) represents a damped signal response to the subthreshold signal since the amplitude of y_3 is $AB/\sqrt{4(1 + \lambda)^2 + \omega^2} \approx A/2$ for $\omega = 2\pi/50$ and $\lambda < \lambda'_1$.

B. Case II: $\lambda \geq \lambda_1$

According to Eq. (10), the signal $AB \sin(\omega t + \phi_1)$ in Eq. (9) turns to suprathreshold at $\lambda = \lambda'_1$, which enables unit three to jump from the initial oscillation center $x_s = -1$ to $x_s = 1$; once unit three enters the area of $x_s = 1$, it becomes completely synchronous with units one and two, forming a cluster. This cluster aggregation process occurs at every site of the ring in a structure like inset (a) in Fig. 5. As a result, the ring transits from spatial asynchronization into two-cluster (clusters I and II) partial synchronization at λ'_1 . Clusters I and II compete for large sizes as the coupling strength λ increases. Due to the contrast inputs from these two clusters, the units at the cluster boundaries fluctuate considerably, leading to a large-amplitude oscillation. This mechanism of cluster synchronization competition accounts for the signal amplification in rings.

Inset (b) in Fig. 5 represents a schematic sketch of the feedforward at λ'_1 , where units one and three belong to cluster I and unit two belongs to cluster II. Because $y_1 \neq y_2$, we get

$$y_1 + y_2 = \frac{4A}{4 + \omega^2} \sin(\omega t) - \frac{2\omega A}{4 + \omega^2} \cos(\omega t). \quad (12)$$

Substituting it into Eq. (6), the dynamics of unit three can be expressed as

$$\dot{y}_3 = (1 - 2\lambda)y_3 - y_3^3 + AB \sin(\omega t + \phi_1). \quad (13)$$

Similarly, the signal $AB \sin(\omega t + \phi_1)$ changes from subthreshold to suprathreshold in Eq. (13) as the coupling strength reaches a threshold λ'_2 . Following Eq. (10), the threshold λ'_2 satisfies

$$\left(\frac{AB}{2}\right)^2 = \left(\frac{1 - 2\lambda'_2}{3}\right)^3. \quad (14)$$

When $A = 0.3$ and $\omega = 2\pi/50$, the threshold $\lambda'_2 \approx 0.06$ which is close to the numerical result $\lambda_2 = 0.09$. Accordingly, the signal $AB \sin(\omega t + \phi_1)$ remains subthreshold for $\lambda'_1 \leq \lambda < \lambda'_2$. Within this coupling interval, the approximated

solution of Eq. (13) can be obtained again by using the linearization method, which takes the form of

$$y_3(t) = \pm\sqrt{1 - 2\lambda} + \frac{AB}{\sqrt{4(1 - 2\lambda)^2 + \omega^2}} \sin(\omega t + \phi_3), \quad (15)$$

where ϕ_3 stands for some phase shift.

When $\lambda \geq \lambda'_2$, the signal $AB \sin(\omega t + \phi_1)$ in Eq. (13) becomes suprathreshold, and unit three starts to oscillate about $x_u = 0$ with a large amplitude. The explanation is that the coupling strength $\lambda \geq \lambda'_2$ greatly promotes the synchronization competition between units one and two, which reduces the potential barrier separating the two fixed points $x_s = \pm 1$ of unit three, turning the subthreshold signal into a suprathreshold signal. To solve Eq. (13), we assume that the frequency ω is so low that the periodic signal acting on unit three can be regarded as a square wave $\pm AB$. With this assumption, the oscillation amplitude I of unit three can be estimated by the real root of the cubic equation $(1 - 2\lambda)y_3 - y_3^3 \pm AB = 0$. If $\lambda'_2 \leq \lambda < 0.5$, the root is

$$I_1 = 2\sqrt{\frac{1 - 2\lambda}{3}} \cosh \left[\frac{1}{3} \operatorname{arcosh} \left(\sqrt{\frac{27A^2B^2}{4(1 - 2\lambda)^3}} \right) \right], \quad (16)$$

and if $\lambda > 0.5$, the root becomes

$$I_2 = 2\sqrt{\frac{2\lambda - 1}{3}} \sinh \left[\frac{1}{3} \operatorname{arsinh} \left(\sqrt{\frac{27A^2B^2}{4(2\lambda - 1)^3}} \right) \right]. \quad (17)$$

Using Eqs. (16) and (17), the solution of Eq. (13) can be expressed as $y_3(t) = I_{1,2} \sin(\omega t)$, i.e., large oscillations about $x_u = 0$.

From Eqs. (11), (15), (16), and (17), we get the analytical signal response of the feed-forward motif as

$$G_{\text{motif}} = \begin{cases} \frac{B}{\sqrt{4(1 + \lambda)^2 + \omega^2}}, & \text{if } \lambda < \lambda'_1, \\ \frac{B}{\sqrt{4(1 - 2\lambda)^2 + \omega^2}}, & \text{if } \lambda'_1 \leq \lambda < \lambda'_2, \\ \frac{I_1}{A}, & \text{if } \lambda'_2 \leq \lambda < 0.5, \\ \frac{I_2}{A}, & \text{if } \lambda > 0.5. \end{cases} \quad (18)$$

Figure 5 shows the prediction of Eq. (18), which agrees well with the result obtained numerically from Eq. (6). Based on Eq. (18), we may estimate the signal response of the ring with $R = 1$ by taking the success rate p into account, yielding

$$G_{\text{ring}} = \begin{cases} G_{\text{motif}}, & \text{if } p = 0, \\ pG_{\text{motif}} + (1 - p)G_{\text{single}}, & \text{if } p > 0. \end{cases} \quad (19)$$

In Fig. 5, we calculate the signal response of Eq. (19) by using the numerical result of p shown in Fig. 3(b). We see that Eq. (19) can better estimate the signal response of the ring with $R = 1$.

V. SUMMARY

In conclusion, we have extended the topological resonance from degree-heterogeneous scale-free networks to degree-homogeneous rings. We have shown that the resonant signal amplification in regular rings is a general phenomenon across a wide range of ring sizes and signal frequencies. Utilizing a three-node feed-forward motif, we have analyzed the resonance mechanism, which agrees well with the numerical result of a ring with local coupling. Here, the mechanism is somewhat different from that of scale-free networks. In scale-free networks, the leaf nodes linked to the hub nodes can be divided into two synchronous clusters according to their initial states. The forcing signal from the global sum of the leaf nodes lowers the effective potential barrier of the hub nodes, enabling the hub nodes to respond substantially to a weak input signal. Thus, the resonance effect of signal amplification in scale-free networks arises from the cooperation between the leaf nodes. In rings with short-distance couplings, two synchronous clusters are formed by the coupling strength. In addition, the two clusters tend to synchronize, causing the nodes located at the cluster boundaries to switch between

clusters. Therefore, the resonant signal amplification in rings results from a competition between cluster synchronization. This competition could be considered a kind of disorder brought about by partial synchronization of the rings with short-distance couplings and intermediate coupling strength. Moreover, unlike scale-free networks where only hub nodes amplify weak signals, all nodes have the same opportunity for signal amplification in rings. Since rings (loops) are prevalent in real networks [45–47], our findings suggest that rings, along with scale-free structures, play essential roles in information processing in networked systems.

ACKNOWLEDGMENTS

X.L. was supported by the NNSF of China under Grant No. 12175087. X.Z. was supported by the NNSF of China under Grant No. 12105117, the Fundamental Research Funds for the Central Universities (Grant No. 21621007), and Guangdong Basic and Applied Basic Research Foundation (Grant No. 2022A1515010523).

-
- [1] A. Pikovsky, M. Rosenblum, and J. Kurths, *Synchronization, A Universal Concept in Nonlinear Sciences* (Cambridge University Press, Cambridge, UK, 2001).
 - [2] M. Konishi, *Sci. Am.* **16**, 28 (2006).
 - [3] S. H. Strogatz, *Nonlinear Dynamics and Chaos: With Applications to Physics, Biology, Chemistry, and Engineering* (Westview Press, Boulder, 2015).
 - [4] M. F. McKenna, *Phys. Today* **73**(1), 28 (2020).
 - [5] L. Gammaitoni, P. Hänggi, P. Jung, and F. Marchesoni, *Eur. Phys. J. B* **69**, 1 (2009).
 - [6] K. Kitajo, D. Nozaki, L. M. Ward, and Y. Yamamoto, *Phys. Rev. Lett.* **90**, 218103 (2003).
 - [7] A. R. Bulsara, *Nature (London)* **437**, 962 (2005).
 - [8] I. Tiwari, J. M. Cruz, P. Parmananda, and M. Rivera, *Phys. Rev. E* **100**, 060202(R) (2019).
 - [9] M. Das and H. Kantz, *Phys. Rev. E* **101**, 062145 (2020).
 - [10] J. K. Douglass, L. Wilkens, E. Pantazelou, and F. Moss, *Nature (London)* **365**, 337 (1993).
 - [11] H. Gang, H. Haken, and X. Fagen, *Phys. Rev. Lett.* **77**, 1925 (1996).
 - [12] L. Gammaitoni, P. Hänggi, P. Jung, and F. Marchesoni, *Rev. Mod. Phys.* **70**, 223 (1998).
 - [13] F. Moss, D. Pierson, and D. O’Gorman, *Int. J. Bifurcation Chaos Appl. Sci. Eng.* **04**, 1383 (1994).
 - [14] P. Hänggi, *Chem. Phys. Chem.* **3**, 285 (2002).
 - [15] D. J. Watts and S. H. Strogatz, *Nature (London)* **393**, 440 (1998).
 - [16] A.-L. Barabási and R. Albert, *Science* **286**, 509 (1999).
 - [17] R. Albert and A.-L. Barabási, *Rev. Mod. Phys.* **74**, 47 (2002).
 - [18] S. Boccaletti, J. A. Almendral, S. Guan, I. Leyva, Z. Liu, I. Sendiña-Nadal, Z. Wang, and Y. Zou, *Phys. Rep.* **660**, 1 (2016).
 - [19] M. Morillo, J. Gómez-Ordoñez, and J. M. Casado, *Phys. Rev. E* **52**, 316 (1995).
 - [20] J. F. Lindner, B. K. Meadows, W. L. Ditto, M. E. Inchiosa, and A. R. Bulsara, *Phys. Rev. Lett.* **75**, 3 (1995).
 - [21] M. Löcher, G. A. Johnson, and E. R. Hunt, *Phys. Rev. Lett.* **77**, 4698 (1996).
 - [22] C. Zhou, J. Kurths, and B. Hu, *Phys. Rev. Lett.* **87**, 098101 (2001).
 - [23] A. Pikovsky, A. Zaikin, and M. A. de la Casa, *Phys. Rev. Lett.* **88**, 050601 (2002).
 - [24] Z. Gao, B. Hu, and G. Hu, *Phys. Rev. E* **65**, 016209 (2001).
 - [25] M. Perc, *Phys. Rev. E* **76**, 066203 (2007).
 - [26] M. Perc, *Phys. Rev. E* **78**, 036105 (2008).
 - [27] Z. Liu and T. Munakata, *Phys. Rev. E* **78**, 046111 (2008).
 - [28] C. J. Tessone, C. R. Mirasso, R. Toral, and J. D. Gunton, *Phys. Rev. Lett.* **97**, 194101 (2006).
 - [29] T. Perez, C. R. Mirasso, R. Toral, and J. D. Gunton, *Phil. Trans. R. Soc. A* **368**, 5619 (2010).
 - [30] M. Patriarca, S. Postnova, H. A. Braun, E. Hernández-García, and R. Toral, *PLoS Comput. Biol.* **8**, e1002650 (2012).
 - [31] C. J. Tessone, A. Sanchez, and F. Schweitzer, *Phys. Rev. E* **87**, 022803 (2013).
 - [32] J. A. Acebrón, S. Lozano, and A. Arenas, *Phys. Rev. Lett.* **99**, 128701 (2007).
 - [33] T. Kondo, Z. Liu, and T. Munakata, *Phys. Rev. E* **81**, 041115 (2010).
 - [34] R. Chacón and P. J. Martínez, *Phys. Rev. E* **92**, 012821 (2015).
 - [35] X. Liang, C. Liu, and X. Zhang, *Phys. Rev. E* **101**, 022205 (2020).
 - [36] X. Liang, X. Zhang, and L. Zhao, *Chaos* **30**, 103101 (2020).
 - [37] S. Boccaletti, V. Latora, Y. Moreno, M. Chavez, and D.-U. Hwang, *Phys. Rep.* **424**, 175 (2006).
 - [38] A. Arenas, A. Díaz-Guilera, J. Kurths, Y. Moreno, and C. Zhou, *Phys. Rep.* **469**, 93 (2008).
 - [39] M. L. Olivera-Atencio, M. Morillo, and J. Casado-Pascual, *Phys. Rev. E* **104**, 064204 (2021).

- [40] F. Lu and Z. Liu, *Chin. Phys. Lett.* **26**, 040503 (2009).
- [41] X. Liang and X. Zhang, *Phys. Rev. E* **104**, 034204 (2021).
- [42] R. Milo, S. Shen-Orr, S. Itzkovitz, N. Kashtan, D. Chklovskii, and U. Alon, *Science* **298**, 824 (2002).
- [43] X. Liang, S. Yanchuk, and L. Zhao, *Phys. Rev. E* **88**, 012910 (2013).
- [44] W. Ding, C. Gu, and X. Liang, *Commun. Theor. Phys.* **65**, 189 (2016).
- [45] S. H. Strogatz, *Nature* **410**, 268 (2001).
- [46] G. Bianconi, N. Gulbahce, and A. E. Motter, *Phys. Rev. Lett.* **100**, 118701 (2008).
- [47] M. E. J. Newman, *Phys. Rev. E* **100**, 012314 (2019).